Title

A basis set for exploration of sensitivity to prescribed ocean conditions for estimating human contributions to extreme weather in CAM5.1-1degree

Authors

Stone, Dáithí A
Risser, Mark D
Angélil, Oliver M
et al.

Publication Date

2018-03-01

DOI

10.1016/j.wace.2017.12.003

Peer reviewed

A basis set for exploration of sensitivity to prescribed ocean conditions for estimating human contributions to extreme weather in CAM5.1-1degree

Dáithí A. Stone[a,*], Mark D. Risser[a], Oliver M. Angélil[a,b], Michael F. Wehner[a], Shreyas Cholia[a], Noel Keen[a], Harinarayan Krishnan[a], Travis A. O'Brien[a], William D. Collins[a]

[a] *Lawrence Berkeley National Laboratory, Berkeley, California, U.S.A.*
[b] *University of New South Wales, Sydney, New South Wales, Australia*

Abstract

This paper presents two contributions for research into better understanding the role of anthropogenic warming in extreme weather. The first contribution is the generation of a large number of multi-decadal simulations using a medium-resolution atmospheric climate model, CAM5.1-1degree, under two scenarios of historical climate following the protocols of the C20C+ Detection and Attribution project: the one we have experienced (All-Hist), and one that might have been experienced in the absence of human interference with the climate system (Nat-Hist). These simulations are specifically designed for understanding extreme weather and atmospheric variability in the context of anthropogenic climate change.

The second contribution takes advantage of the duration and size of these simulations in order to identify features of variability in the prescribed ocean conditions that may strongly influence calculated estimates of the role of anthropogenic emissions on extreme weather frequency (event attribution). There is a large amount of uncertainty in how much anthropogenic emissions should warm regional ocean surface temperatures, yet contributions to the C20C+ Detection and Attribution project and similar efforts so far use only one or a limited number of possible estimates of the ocean warming attributable to anthropogenic

*Corresponding author

emissions when generating their Nat-Hist simulations. Thus, the importance of the uncertainty in regional attributable warming estimates to the results of event attribution studies is poorly understood. The identification of features of the anomalous ocean state that seem to strongly influence event attribution estimates should therefore be able to serve as a basis set for effective sampling of other plausible attributable warming patterns. The identification performed in this paper examines monthly temperature and precipitation output from the CAM5.1-1degree simulations averaged over 237 land regions, and compares interannual anomalous variations in the ratio between the frequencies of extremes in the All-Hist and Nat-Hist simulations against variations in ocean temperatures.

Keywords: C20C+ D&A, CAM5.1, extremes, event attribution, attributable warming

---

1. Toward tackling a major uncertainty in event attribution analysis

The field of research investigating the role of anthropogenic emissions in specific extreme weather events (termed "event attribution" in the remainder of this paper) has gained interest in recent years but is still in an early stage of development (Stott et al., 2013; National Academies of Sciences, Engineering, and Medicine, 2016). At this stage, there are a considerable (and growing) number of methods being used, some with rather different philosophical underpinnings (Shepherd, 2016). One of the most popular methods compares the frequency of exceedance of some threshold in simulations of a dynamical atmospheric model driven under a factual scenario of observed radiative and surface boundary conditions against the frequency in simulations driven under a counterfactual scenario of what those boundary conditions might have been like in the absence of human interference with the climate system (Pall et al., 2011). Conclusions of studies using this atmospheric-modelling time-slice approach are usually expressed numerically in terms of the Risk Ratio or Fraction Attributable Risk (Stone and Allen, 2005). This type of experiment is explic-

itly supported by the design of the Climate of the 20th Century Plus Detection and Attribution (C20C+ D&A) Project, the topic of the special journal issue in which this paper appears (Stone et al., In preparation).

A consequence of the relative youthful stage of this research field, however, is that a number of aspects of the experiment design remain poorly understood in terms of the potential generation of bias and quantification of uncertainty (National Academies of Sciences, Engineering, and Medicine, 2016). For the atmospheric-modelling time-slice approach, possibly the biggest uncertainty involves generation of the estimate of ocean warming (and sea ice retreat) attributable to anthropogenic emissions. There are a number of plausible approaches to estimating the attributable warming, including approaches based on observed trends (Christidis and Stott, 2014), approaches based on simulations of dynamical models of the coupled atmosphere-ocean system (Pall et al., 2011; Christidis et al., 2012; Shiogama et al., 2014; Wolski et al., 2014; Schaller et al., 2016; Stone and Pall, 2017), and approaches that combine climate models and observations (Bichet et al., 2015, 2016). Estimates based on observed trends suffer from poor sampling, and thus a large amount of the estimated pattern of attributable warming consists of random endogenously generated variability rather than a response signal to an external forcing; because extreme weather tends to feed off of local temperature gradients, such "noise" may have an important influence on event attribution results. Estimates based on atmosphere-ocean climate models may be better sampled (Stone and Pall, 2017), but they depend on usage of accurate estimates of the drivers of climate change as well as on the capability of atmosphere-ocean climate models to accurately represent the effect of those drivers on ocean surface conditions. Only a few of the many studies so far using the atmospheric-modelling time-slice approach have used multiple estimates of the counterfactual natural scenario based on various attributable ocean warming estimates (Pall et al., 2011; Kay et al., 2011; Christidis et al., 2012; Shiogama et al., 2014; Christidis and Stott, 2014; Schaller et al., 2016), and even these have used a miniscule number in relation to the enormous size of the space of possible values.

Considering the computational cost of running the simulations, the viability of the atmospheric-modelling time-slice approach to event attribution depends on the ability to reduce the size of the space of attributable ocean warming estimates to a manageable number. A first step toward this is the assumption of separability into a spatio-temporal pattern and scalar global amplitude (Pall et al., 2011). The linearity of event attribution results for extreme autumn seasonal precipitation over England-Wales (Pall et al., 2011) and extreme local daily precipitation within South Africa (Angélil et al., 2014) as a function of the global amplitude parameter suggests that this may be a reasonable assumption. The pattern-amplitude separation not only substantially reduces the total size of the attributable warming space, but it also effectively solves the bias and uncertainty estimation issues for the amplitude half of the attributable warming problem, because this is accurately constrained by long-term historical global warming (Stott et al., 2006; Pall et al., 2011). Note that the separation considered here differs from that proposed in Bichet et al. (2015, 2016), which instead separates in spatial and temporal components.

The assumption of pattern-scalar separability thus transforms the problem of attributable warming estimation into a problem of spatio-temporal pattern estimation. We are still left with an effectively infinite number of possible patterns, however, so some further efficiency is required. One option, labeled here as the "available pattern approach", is to sample whatever pattern estimates are available (e.g. Pall et al., 2011; Schaller et al., 2016). A more complete sampling of the same space of available estimates might be achieved through cluster analysis (Mizuta et al., 2014). The advantage is that the patterns are plausible responses to anthropogenic forcing (notwithstanding errors in observational data and biases in climate models). The disadvantage however is that there is no obvious reason why the space spanned by the relatively few patterns should be strongly aligned with the directions of high sensitivity of event attribution results; thus, these few patterns may provide a poor indication of the sensitivity to plausible patterns that have not been sampled. One might imagine for instance that a set of available attributable ocean warming patterns differs only in the

equator-to-pole gradient, while for a tropical region uncertainty in the risk ratio depends only on uncertainty in the interhemispheric gradient. Thus a second option, proposed here and labeled the "sensitivity-based approach", is to instead focus on sampling patterns corresponding to the directions of highest sensitivity of event attribution results. The disadvantage of this second approach is that is unclear whether such patterns are plausible responses to anthropogenic forcing. The two approaches are thus complementary.

This paper sets out to facilitate sampling of the uncertainty in the attributable ocean warming pattern by further reducing the space of useful patterns to a manageable number using the sensitivity-based approach. We identify the directions of attributable warming with the highest sensitivity in event attribution results, with these directions being perturbations from the baseline attributable warming estimate (Stone and Pall, 2017) used by the C20C+ D&A project. To do so, we examine the year-to-year sensitivity of risk ratio estimates for monthly extremes to interannual variability in sea surface temperatures (Risser et al., 2017), using a set of large ensembles of multi-decadal simulations of an atmospheric climate model. We start by describing the simulations in detail, including specifics of the experiment setup. We then describe the method used to identify sensitivity to anomalous sea surface temperature variability, and develop its application here to the identification of a subspace of patterns to which risk ratio estimates for events around the world are generally most sensitive.

2. Simulations of CAM5.1-1degree

In this section we describe the simulations of the CAM5.1-1degree model of the atmosphere/land system submitted to the C20C+ D&A Project. These simulations are unusual in the combination of their number and duration, properties required for the study described in this paper. Because the C20C+ D&A experiment protocol permits some flexibility, it may be useful to spell out the specifics of these simulations here.

2.1. The CAM5.1-1degree model

CAM5.1 is the atmospheric component of the CESM1.0.3 earth system model (Neale et al., 2012). Here it is run at $1.25° \times 0.9375°$ resolution in longitude and latitude respectively (hence the "1degree" suffix in our label for the model), with 30 vertical hybrid height-pressure levels. The dynamical equations are solved using the finite volume (FV) dynamical core. In our configuration, we also use CLM4.0 (Oleson et al., 2010; Lawrence et al., 2011), the model of land surface properties in CESM1.0.3. Chemistry and ecosystem properties are not simulated in either the atmosphere or land models, but rather prescribed for computational efficiency.

2.2. Scenarios

The model has been run under the two benchmark scenarios of the C20C+ D&A project: All-Hist/est1, and Nat-Hist/CMIP5-est1 (Stone et al., In preparation; Stone and Pall, 2017). The collection of simulations of CAM5.1-1degree described in this paper are labeled "All-Hist/est1/v2-0" and "Nat-Hist/CMIP5-est1/v2-0" respectively, with the "v2-0" distinguishing from some trial All-Hist/est1/v1-0 simulations which have some differences in the radiative forcing and are not considered in this paper. The All-Hist/est1/v2-0 simulations are intended to represent possible trajectories for the atmosphere (and land surface) under observed boundary conditions; the Nat-Hist/CMIP5-est1/v2-0 simulations are intended to represent possible trajectories of the atmosphere under an estimate of what the observed boundary conditions might have been in the absence of anthropogenic interference with the climate system. 400 simulations have been run under each scenario, with start dates on 1 January 1959, 1996, or 2010 (Table 1). All simulations start from the same initial state, except for small uniform perturbations applied to the three-dimensional temperature field (note that some simulations listed as starting on 1 January 1959 actually start a year earlier). For this study we ignore the first year of each simulation in order to ensure sufficient divergence from the common initial macrostate.

Table 1: Lengths of simulations as of 30 June 2017. Continued extension of the end date of all simulations is planned as observed sea surface temperature and sea ice concentration data become available.

Scenario	**Simulations**	**Period covered**
All-Hist/est1/v2-0	50	1959/01/01–2016/12/31...
	50	1996/01/01–2016/12/31...
	300	2010/01/01–2013/12/31...
Nat-Hist/CMIP5-est1/v2-0	50	1959/01/01–2015/06/30...
	50	1996/01/01–2015/06/30...
	300	2010/01/01–2013/12/31...

2.3. Experiment setup

The All-Hist/est1/v2-0 simulations have been driven with observed (or observationally-derived) changes in greenhouse gas concentrations, sulphate aerosol burden, organic aerosol burden, black carbon aerosol burden, dust aerosol burden, sea salt aerosol burden, ozone concentrations, solar insolation, volcanic aerosol, land surface cover/use, sea surface temperatures (SSTs), and sea ice concentrations (SICs) (Table 2 and references therein). Prescribed modal aerosol values are used for the non-volcanic aerosols; volcanic aerosols are prescribed through a height-latitude profile of the mass mixing ratio. The consequence of not using prescribed aerosol emissions, and not simulating atmospheric chemistry, is a topic for planned future research.

The Nat-Hist/CMIP5-est1/v2-0 simulations mimic the All-Hist/est1/v2-0 in many ways, but with adjustments to represent the effect of removing the historical influence of anthropogenic emissions (Table 2 and references therein). Solar and volcanic forcing is identical to All-Hist/est1/v2-0. However, values for greenhouse gas concentrations, aerosol burdens, and ozone concentrations are held at estimated year 1855 values. SSTs from All-Hist/est1/v2-0 are cooled according to the "Nat-Hist/CMIP5-est1" monthly estimate of attributable warming from Stone and Pall (2017). This estimate of the warming attributable to human interference with the climate system is calculated as the difference between

Table 2: Radiative and surface boundary conditions used in the All-Hist/est1/v2-0 and Nat-Hist/CMIP5-est1/v2-0 simulations performed with CAM5.1-1degree. CFC-11 values are adjusted in order to represent a number of species: CFC-11, CCl_4, CF_4, C_2F_6, C_6F_{14}, CH_3Br, CH_3Cl, CFC-113, CFC-114, CFC-115, Halon-1211, Halon-1301, Halon-2402, HCFC-22, HCFC-141B, HCFC-142B, HFC-23, HFC-32, HFC-43-10, HFC-125, HFC-134a, HFC-143a, HFC-227ea, HFC-245fa, methyl chloroform, SF_6. Aerosols include: black carbon, dust, organic, sulphate, and sea salt. Year 1855 values for Nat-Hist/CMIP5-est1/v2-0 involve repeating the annual cycle from that year.

Boundary condition	**All-Hist/est1/v2-0**	**Nat-Hist/CMIP5-est1/v2-0**
CO_2	Prescribed from Meinshausen et al. (2011)	284.725ppmv
CH_4	Prescribed from Meinshausen et al. (2011)	790.979ppbv
N_2O	Prescribed from Meinshausen et al. (2011)	275.425ppbv
CFC-11	Prescribed from Meinshausen et al. (2011)	33.432pptv
CFC-12	Prescribed from Meinshausen et al. (2011)	0.0pptv
Sulphate aerosol	Prescribed modal aerosol from Lamarque et al. (2012)	Year 1855 prescribed modal aerosol from Lamarque et al. (2012)
Black carbon aerosol	Prescribed modal aerosol from Lamarque et al. (2012)	Year 1855 prescribed modal aerosol from Lamarque et al. (2012)
Organic aerosol	Prescribed modal aerosol from Lamarque et al. (2012)	Year 1855 prescribed modal aerosol from Lamarque et al. (2012)
Dust aerosol	Prescribed modal aerosol from Lamarque et al. (2012)	Year 1855 prescribed modal aerosol from Lamarque et al. (2012)
Sea salt aerosol	Prescribed modal aerosol from Lamarque et al. (2012)	Year 1855 prescribed modal aerosol from Lamarque et al. (2012)
Ozone	Lamarque et al. (2010) and Lamarque et al. (2011)	Year 1855 from Lamarque et al. (2010) and Lamarque et al. (2011)
Solar luminosity	Wang et al. (2005)	Wang et al. (2005)
Volcanic aerosol	Ammann et al. (2003)	Ammann et al. (2003)
Land surface	Hurtt et al. (2006)	Hurtt et al. (2006)
Sea surface temperature	Hurrell et al. (2008) and NOAA OI.v2 (Reynolds et al., 2002)	Hurrell et al. (2008) and NOAA OI.v2 (Reynolds et al., 2002) adjusted according to Stone and Pall (2017)
Sea ice concentration	Hurrell et al. (2008) and NOAA OI.v2 (Reynolds et al., 2002)	Hurrell et al. (2008) and NOAA OI.v2 (Reynolds et al., 2002) adjusted according to Stone and Pall (2017)

the "historical" (drivern with historical changes in both anthropogenic and natural forcings) and "historicalNat" (driven with historical changes in natural forcings only) simulations from the Coupled Model Intercomparison Project Phase 5 (CMIP5, Taylor et al., 2012). Sea ice concentrations are adjusted for consistency with the cooler temperatures according to the observed temperature-ice relationship (Stone and Pall, 2017). Visuals illustrating the spatial and temporal properties of the resulting All-Hist/est1 and Nat-Hist/CMIP5-est1 SSTs and sea ice coverage are provided in Stone and Pall (2017). Additionally, the data is available for download at http://portal.nersc.gov/c20c/.

The C20C+ D&A protocols are flexible in terms of whether land use/cover change is considered a global or local anthropogenic forcing, and thus whether it is a driver of change which the benchmark Nat-Hist/CMIP5-est1 scenario is intended to diagnose. For the CAM5.1-1degree Nat-Hist/CMIP5-est1/v2-0 simulations we have interpreted it as a local forcing for the purposes of extreme weather, and thus not something to be diagnosed in this global experiment. Therefore, the All-Hist/est1/v2-0 land use/cover change is retained for the Nat-Hist/CMIP5-est1/v2-0 simulations. The effect of this choice is a topic of planned future research.

Further details on these simulations are available at http://portal.nersc.gov/c20c/data.html, including on planned continual updates as observed SSTs and SICs become available.

3. Method

The experimental design used in the C20C+ simulations involves some important assumptions relating to the ocean surface state and the way the atmosphere interacts with the ocean. In order to assess the impact of ocean variability on atmosphere-model-based event attribution, Risser et al. (2017) develop a hierarchical statistical model that allows for quantification of the uncertainty introduced in attribution studies from the use of uncoupled, atmosphere/land-only model simulations (in addition to sampling uncertainty from the limited

number of simulations). Specifically, the framework provides a way to quantify the effect of ocean variability on the risk ratio, while taking account of the effect of long-term trends.

For complete details of the statistical approach, we refer the reader to the methods section of Risser et al. (2017); however, a summary is as follows. Given the long term nature of the CAM5.1-1degree simulations, we are interested in estimating the risk ratio over time at a total of T years, i.e.,

$$RR_t = \frac{p_{At}}{p_{Nt}} \qquad t = 1, \ldots, T,$$

where p_{At} and p_{Nt} are the occurrence probabilities for a defined extreme event in year t for scenario All-Hist and Nat-Hist, respectively. Together with a non-parametric (or binomial) likelihood, the scenario-specific probabilities for each calendar month are modeled using mixed-effects logistic regression as

$$\log\left(\frac{p_{ktj}}{1-p_{ktj}}\right) = \beta_{k0} + \beta_{k1}x_{kt} + \alpha_t + \delta_t 1_{\{k=A\}} + \gamma_j, \tag{1}$$

for $k \in \{A, N\}$, $j \in \{1, \ldots, 12\}$ (an index for the calendar months), and $t = 1, \ldots, T$. While calculations are performed with the γ_j seasonality term included, for simplicity we take annual averages over the resulting seasonality in this paper when presenting results for δ_t, p_{At}, p_{Nt}, and RR_t and we will drop the j index in the remainder of this summary of the method. Here, x_{kt} is a time-varying covariate for scenario $k \in \{A, N\}$ (we use a smoothed scenario-specific 50°S-50°N land annual mean temperature), β_{k0} and β_{k1} are scenario-specific regression coefficients, and $1_{\{\cdot\}}$ is an indicator function. Intuitively, including the scenario-specific covariate accounts for any long-term trends present in p_N and p_A. Then, we use a prior for the α_t and δ_t that borrows information across years, which is a standard form of statistical shrinkage that increases the signal to noise ratio when estimating these effects. The choice of priors does not affect the best estimate of the long-term trend itself, but rather encourages a decrease in the uncertainty in the trend. The statistical model is estimated in a Bayesian framework, using Markov chain Monte Carlo (MCMC) methods to obtain joint samples from the posterior distribution, upon which all subsequent inference

is based. We assume that all values are independent in time, which is reasonable for the monthly mean data (admittedly notwithstanding some intra-annual variability that is not accounted for by the t index) examined in this paper but would not be for daily frequencies.

Using (1) for p_{At} and p_{Nt}, the risk ratio in year t is approximately

$$RR_t \approx RR_0 \times \exp\{\beta_{A1} x_{At1} - \beta_{N1} x_{Nt1}\} \times \exp\{\delta_t\}.$$

Thus, $RR_0 = \exp\{\beta_{A0} - \beta_{N0}\}$ is the "baseline" risk ratio for the entire time interval, a scalar that centres the analysis on a particular climate era (and means that the approximation is not valid for a period experiencing a large amount of climate change in either scenario). The $\exp\{\beta_{A1} x_{At1} - \beta_{N1} x_{Nt1}\}$ term, a multiplicative scaling due to the covariates, describes the long term trend in the risk ratio, where the trend is taken to have the form of the difference in the global mean temperature covariates of the two scenarios. Finally, the $\exp\{\delta_t\}$ term is a scaling for the risk ratio in a particular year that describes the year-to-year variability in the p_{At} above and beyond variability in the p_{Nt} (after accounting for long term trends in the probabilities due to atmospheric warming). Hence, the δ_t effects also describe the year-to-year variability in the risk ratio beyond the long term trend, and are of particular interest to our analysis in the next section. Together the first two terms describe the mean anthropogenic effect as measured by the risk ratio; the δ_t term describes anomalous year-to-year variations in that anthropogenic effect that result from the anomalous ocean state modulating the way that the climate system interprets the anthropogenic forcing.

In order to account for regional differences in the probabilities p_{At} and p_{Nt} and hence the δ_t, we fit the statistical model to area-averaged monthly output from the simulations for each of 237 diagnostic land regions (Stone, 2017, , see Figure 5) over the 1982-2014 period. For hot, cold, and wet extremes, we then have an estimated time series of the δ_t (33 total years) for each of the 237 regions. The focus on monthly extremes is motivated in part because these may be expected to be more sensitive to prescribed ocean conditions than shorter-

duration events. Given that risk ratios tend to scale straightforwardly as a function of duration and spatial scale (Angélil et al., 2017), the results here should be qualitatively relevant for hot, cold, and wet extremes for different durations and regions than are examined here.

4. Results

4.1. Year-to-year variability in extreme weather probabilities

As an example, Figure 1 shows the estimated probabilities of hot, cold, and wet months over the U.S. states of California and Nevada (comprising one of the 237 diagnostic regions) for each year in the 1982-2014 period under both scenarios. We do not examine dry months because over many regions, such as this one, a zero-precipitation month can be fairly common. Thresholds are defined as the 1-in-10-year event over the 1982-2014 period in the All-Hist/est1/v2-0 simulations. While the probabilities of a hot month were similar between the two scenarios in the 1980s, they are at least five times more probable in recent years. In contrast, the probabilities of cold months are already about three times lower in All-Hist/est1/v2-0 scenario in the 1980s, with only a slight further increase in the probabilities in recent years. Probabilities of wet months are similar between the two scenarios.

Along with long-term trends in the probabilities plotted in Figure 1, there are also notable interannual variations. For instance, the probability of a wet month is substantially higher in 1983 and 1998 under both scenarios: both years experienced strong El Niño events which often induce wet winters over this region. However, the variations are not identical across the two scenarios. For instance, even though the estimated probabilities appear to be higher in both 1983 and 1998 with anthropogenic forcing, the highest estimated probability of a wet month in the Nat-Hist/CMIP5-est1/v2-0 scenario is in 1998, while it is 1983 for the All-Hist/est1/v2-0 scenario. Some of these variations represent uncertainty from the limited sample of simulation data available, however Risser et al. (2017) concluded that some of the differences represent real features of the

anthropogenic influence on extreme weather, at least as represented by CAM5.1-1degree.

4.2. Correlation of risk ratio with sea surface temperatures

In order to achieve the goal of this paper, we would like to diagnose what spatial patterns of SST variability might be related to the year-to-year variations in the differences in probabilities between the two scenarios, beyond long-term global warming. In other words, what SST patterns are responsible for the year-to-year variability in the risk ratio estimates? We measure these variations in the risk ratio using the δ_t effects introduced in Section 3. This variable represents variations in the risk ratio beyond those from mean global warming, with the risk ratio being the probability under the All-Hist/est1/v2-0 scenario divided by the probability under the Nat-Hist/CMIP5-est1/v2-0 scenario (Stone and Allen, 2005). We then calculate the linear correlation between the estimated δ_t and the year-to-year variations in SST at each location in the ocean (across 1982-2014). The result is plotted in Figure 2 for the case of wet months over California and Nevada.

The year-to-year variability in the risk ratio for wet months over California and Nevada is correlated with SSTs in the Pacific Ocean, in patterns that resemble the El Niño/Southern Oscillation (ENSO) phenomenon in the tropical Pacific and the Pacific Decadal Oscillation (PDO) in the extratropical North Pacific. These phenomena are known to influence precipitation over California and Nevada (Dettinger et al., 2011). Their visibility in these maps, however, suggests that the extent of their influence may depend on the existence of anthropogenic forcing. Stated differently, the existence of an El Niño-like pattern in this map suggests that during El Niño events extreme wet months over California and Nevada become wetter under anthropogenic forcing than would be expected based on the anthropogenic effect on ENSO-neutral months. We need to be careful not to overinterpret that suggestion though. First, because wet months are more probable over these states in years when there is an El Niño event occurring, the anomalous risk ratio correlation map is sensitive to the lim-

ited sampling of those El Niño months; a similar issue exists for PDO phases. Second, the correlations are not that strong, ranging from -0.59 to 0.61, or about one third of the variance being shared at a maximum.

4.3. Global patterns of anomalous variability in regional risk ratios

While anomalous year-to-year variations in the estimated risk ratio (δ_t) for California and Nevada may be correlated with the PDO, this may not be the case with the other 236 regions. In order to collectively analyse all regions, we perform a principal component (PC) analysis on the estimated δ_t variable across all regions and years in the 1982-2014 period (the principal components are calculated based on the correlation matrix of the δ_t). Because all regions are approximately the same size by design, we do not apply any area-based weighting. The normalised eigenvalues are plotted in Figure 3 separately for hot, cold, and wet events. Slightly more PCs are required to represent 90% (red line) of the anomalous variability in the risk ratio of hot events than for cold events, while nearly twice as many PCs are required for wet events as for cold events. This difference might be expected given that temperature variability has a larger spatial decorrelation scale than does precipitation variability (Jones et al., 1997).

The leading PC related to cold events represents nearly half of the anomalous variability in the risk ratio, while the leading PC for hot and wet events represents about a quarter and a fifth of the variance respectively. The PC time series are ploted in Figure 4, with the associated spatial projections plotted in Figure 5.

The leading PC for cold events marks the occurrence of El Niño events, with the lowest four values corresponding to four of the top five El Niños of the period: the 1983, 1987, 1998, and 2010 events. The spatial projection indicates that when there is an El Niño event (negative) tropical land regions have an anomalously high risk ratio. If this PC is reflecting an effect of ENSO variations on the risk ratio, then it might be expected to be strongly correlated with SSTs in the tropical Pacific. Figure 6 shows the map of the correlation

between annual mean SSTs and the time series associated with the leading PC. Note that this map is not actually showing the PC, which is based on the anomalous risk ratio variability of the 237 land regions. The SST correlation map for the anomalous risk ratio of cold events resembles the PDO (Mantua et al., 1997), with correlations ranging between -0.71 and 0.73 in the Pacific Ocean. However, there is no strong correlation visible in the tropical Pacific itself, i.e. with ENSO variability. The explanation would seem to be that the leading PC is reflecting the effect of the El Niño phase of ENSO but not of the opposite La Niña phase: this nonlinear relationship is not being picked up by a linear correlation. Tropical land regions have a lower probability of a cold month during an El Niño (also known as "warm ENSO") event, which makes them almost impossible in the Nat-Hist/CMIP5-est1 world but merely less likely in the All-Hist world (not shown), resulting in a substantially higher risk ratio; in contrast, a La Niña event does not lead to a near-zero numerator or denominator in the risk ratio.

The leading PC for the anomalous risk ratio of hot events generally represents opposite behaviour in the tropics versus the non-tropics. The correlation with SSTs shows a similar pattern, with in-phase correlations in the tropical Pacific, tropical North Atlantic, and the Indian Ocean. However, the correlations with SSTs are generally weaker than for cold or wet events. In the Indian Ocean the pattern resembles the Indian Ocean Dipole (IOD), but correlations between the Dipole Mode Index of the IOD (Saji and Yamagata, 2003) and the anomalous risk ratio time series of individual regions only span the -0.58 to 0.40 range, so this probably does not reflect anything substantial.

For wet events, the leading PC for the anomalous variability in the risk ratio mostly represents a long-term linear trend until around 2005, with no trend over the final decade. Its spatial projection mainly focuses on the northern half of Africa. It may represent a simulated version of the recovery of the Sahel (and here surrounding areas) rainfall since the drought of the early 1980s. This area generally has a lower chance of wet events in the All-Hist/est1/v2-0 simulations. Thus, as the frequency of wet events increases during this period, the shift in the

distribution has a larger effect on All-Hist events, increasing their probability by about a factor of five while the probability in the Nat-Hist/CMIP5-est1 simulations merely doubles (not shown). The correlation of the PC with SSTs is strongly focused on the North Atlantic (reaching values as high as 0.91), a region that has been linked to the recovery of the Sahel rains (Hoerling et al., 2006).

5. Application for alternative natural ocean surface estimates

Uncertainty in what the ocean surface might have been like in the absence of anthropogenic interference is probably the largest uncertainty in the popular time-slice atmospheric modelling approach to event attribution first presented by Pall et al. (2011) and adopted by the C20C+ D&A project Stone et al. (In preparation). One can generate a plausible estimate, as for instance the Nat-Hist/CMIP5-est1 SSTs used as the benchmark natural-SST estimate for the C20C+ D&A project (Stone and Pall, 2017), but there exists an essentially infinite number of perturbations to such a natural-world SST estimate that could be just as plausible. How can we effectively sample across that uncertainty?

In this paper we have developed and presented the maps in Figure 6 as possible anomalous patterns in attributable warming to which estimates of the risk ratio of extreme weather may be highly sensitive. The idea has been that areas of particularly high amplitude correlation in the maps are areas to which the risk ratio (or a similar measure of attributable influence) is most sensitive. For instance, there appears to be a large number of regions for whom the estimate of the risk ratio of wet months is sensitive to SSTs in the North Atlantic Ocean, because the correlation values are particularly high for the leading principal component shown in Figure 6. The sensitive land regions tend to be located in the northern subtropics, with a particular focus on the northern half of Africa (Figure 5). The sensitivity patterns in Figure 6 are based on a particular estimate of the ocean warming attributable to anthropogenic emissions and thus specifically represent directions from that pattern for which risk ratio estimation

may be most sensitive. Whether similar anomalous patterns would be developed when using another baseline attributable warming estimate is an open question which requires the generation of a similarly large ensemble of simulations of CAM5.1-1degree or another model under a different Nat-Hist scenario.

Of course there are a number of questions concerning how these patterns can best be used. In terms of implementation, what magnitude would be most appropriate? This could be an arbitrary ratio of the variance of that pattern in the observed SST record. Alternatively it could be based on the spread of multiple existing attributable warming estimates. For instance, one could calculate attributable warming estimates from multiple individual CMIP5 models (e.g. Schaller et al., 2016), project the sensitivity patterns onto the multiple estimates, and estimate appropriate amplitudes based on the spread of these projections. Alternatively the multiple attributable warming estimates could be expressed as anomalies from a baseline estimate (such as the Nat-Hist/CMIP5-est1 attributable warming estimate used here), the multiple estimates could be ranked according the magnitude of the correlation of these anomalous patterns with the sensitivity patterns, and that ranking could be used to provide prioritisation of the sampling of the multiple existing estimates. Indeed, using these patterns as a means to more efficiently sample between existing available estimates may represent the most effective use of both the available estimates and these sensitivity patterns.

6. Conclusions

This paper has described the generation of an unusually numerous and lengthy set of simulations designed for investigation of extreme weather and climate variability within the context of climate change, following the protocols of the C20C+ D&A project. The C20C+ D&A project currently includes half-century-long simulations under both the All-Hist/est1 and Nat-Hist/CMIP5-est1 scenarios for two additional atmospheric climate models (HadAM3P-N96 and HadGEM3-A-N216), but the ensemble sizes for the CAM5.1-degree simula-

tions described here are considerably larger (Stone et al., In preparation). The "d4PDF" experiment with the MRI-AGCM3.2 model is comparable, being run at a somewhat higher spatial resolution and involving ensemble sizes twice as large for the full multi-decadal period (Shiogama et al., 2016). Considering that the d4PDF "natural" world is estimated using a different, observationally-based, attributable warming estimate than is used here for CAM5.1-1degree, repetition of the analysis conducted here with d4PDF simulations would provide an indication of the robustness of results to both climate model and attributable warming estimate.

Multi-decadal simulations with atmosphere-ocean models run under "historical" and "natural historical" scenarios are also available, for instance through CMIP5 (Taylor et al., 2012), and the relatively small ensemble sizes can be mitigated by use of multiple years in a given era. Coupled atmosphere-ocean models include long-time-scale variability generated by the ocean, which may be relevant in some regions (Risser et al., 2017), but they can also suffer from substantial biases that can be reduced when observed ocean conditions are prescribed (notwithstanding observational errors). Coupled models also include short-time-scale coupling that may be important for tropical cyclone dynamics (Dong et al., 2017). However, in order to accurately simulate tropical cyclones, climate models need to be run at a spatial resolution that in CMIP5 was well beyond what was feasible for a large ensemble of multi-decadal simulations (Wehner et al., 2015). Thus, experiments with atmospheric models such as those here provide a complementary, and in some cases likely more accurate, tool for understanding extreme weather in the context of anthropogenic climate change.

When atmospheric models are used in factual-counterfactual experiments for diagnosing the effect of anthropogenic emissions, uncertainty in how the ocean might respond to anthropogenic emissions is separated from the dynamical modelling apparatus. Instead, the ocean warming to emissions is prescribed. Thus, the uncertainty that might be characterised by using multiple atmosphere-ocean models is now split between using multiple atmospheric models and multiple es-

timates of the attributable ocean warming. Sampling these ocean warming estimates can be undertaken in essentially the same method as when using multiple atmosphere-ocean models: simply sample directly from individual atmosphere-ocean models. However, once the attributable ocean warming has been separated from the dynamical modelling, other possible estimates become available, such as observed trends (e.g. Christidis and Stott, 2014; Bichet et al., 2015). The capability to sample beyond estimates from the limited number of available atmosphere-ocean models and (very limited) observations would thus mean that in one respect atmosphere-only experiments may paradoxically provide improvements over atmosphere-ocean models in terms of how the ocean response is represented.

In this paper, we have proposed a method, based on the CAM5.1-1degree ensembles, that can allow such further sampling of possible natural-world ocean climates. Besides technical limitations involving assumptions and approximations in the methodology, as described in Section 3, there are also practical and existential questions. On the practical side, how might we limit the selection of possible attributable warming estimates to physically plausible ones? One option proposed above, using the basis set developed here to interpolate between single estimates generated through other approaches, has the drawback that it contradicts the main justification of the development of this method: to go beyond the range spanned by those other approaches. A sensitivity-based approach, in which extreme cases are studied in order to understand where the main uncertainties lie, may be a more useful implementation. Nevertheless, the ultimate usefulness depends on the existential question of whether sensitivity to year-to-year variability in the risk ratio of these experiments projects substantially onto the space of plausible attributable warming patterns.

While this paper only analysed monthly data from the CAM5.1-1degree simulations, daily and 3-hourly output is also available through the C20C+ D&A project data portal at http://portal.nersc.gov/c20c/data.html. Along with being applicable to "one-off" attribution studies, most appropriately with other C20C+ D&A models or other data sources, the number and length of the sim-

ulations permit systematic analyses that may help us better understand the time-slice modelling approach from a technical perspective, as well as the global role of anthropogenic interference in local extremes.

References

Ammann C. M. Meehl GA, Washington WM, Zender C. A monthly and latitudinally varying volcanic forcing dataset in simulations of 20th century climate. Geophys Res Lett 2003;30. doi:10.1029/2003GL016875.

Angélil O, Stone D, Wehner M, Paciorek CJ, Krishnan H, Collins W. An independent assessment of anthropogenic attribution statements for recent extreme temperature and rainfall events. J Climate 2017;30:5–16. doi:10.1175/JCLI-D-16-0077.1.

Angélil O, Stone DA, Pall P. Attributing the probability of South African weather extremes to anthropogenic greenhouse gas emissions: spatial characteristics. Geophy Res Lett 2014;41:3238–43. doi:10.1002/2014GL059760.

Bichet A, Kushner PJ, Mudryk L. Estimating the continental response to global warming using pattern-scaled sea surface temperatures and sea ice. J Climate 2016;29:9125–39. doi:10.1175/JCLI-D-16-0032.1.

Bichet A, Kushner PJ, Mudryk L, Terray L, Fyfe JC. Estimating the anthropogenic sea surface temperature response using pattern scaling. J Climate 2015;28:3751–63. doi:10.1175/JCLI-D-14-00604.1.

Christidis N, Stott PA. Change in the odds of warm years and seasons due to anthropogenic influence on the climate. J Climate 2014;27:2607–21.

Christidis N, Stott PA, Zwiers FW, Shiogama H, Nozawa T. The contribution of anthropogenic forcings to regional changes in temperature during the last decade. Clim Dyn 2012;39:1259–74. doi:10.1007/s00382-011-1184-0.

Dettinger MD, Ralph FM, Das T, Neiman PJ, Cayan DR. Atmospheric rivers, floods and the water resources of California. Water 2011;3:445–78. doi:10.3390/w3020445.

Dong B, Sutton RT, Shaffrey L, Klingaman NP. Attribution of forced decadal climate change in coupled and uncoupled ocean-atmosphere model experiments. J Climate 2017;doi:10.1175/JCLI-D-16-0578.1.

Hoerling M, Hurrell J, Eischeid J, Phillips A. Detection and attribution of twentieth-century northern and southern African rainfall change. J Climate 2006;19:3989–4008.

Hurrell JW, Hack JJ, Shea D, Caron JM, Rosinski J. A new sea surface temperature and sea ice boundary dataset for the Community Atmosphere Model. J Climate 2008;21:5145–53.

Hurtt GC, Frolking S, Fearon MG, Moore B, Shevliakova E, Malyshev S, Pacala SW, Houghton RA. The underpinnings of land-use history: three centuries of global gridded land-use transitions, wood-harvest activity, and resulting secondary lands. Global Change Biol 2006;12:1208–29.

Jones PD, Osborn TJ, Briffa KR. Sampling errors in large-scale temperature averages. J Climate 1997;10:2548–68.

Kay AL, Crooks SM, Pall P, Stone DA. Attribution of Autumn/Winter 2000 flood risk in England to anthropogenic climate change: a catchment-based study. J Hydrol 2011;406:97–112. doi:10.1016/j.jhydrol.2011.06.006.

Lamarque JF, Bond TC, Eyring V, Granier C, Heil A, Klimont Z, Lee D, Liousse C, Mieville A, Owen B, Schultz MG, Shindell D, Smith SJ, Stehfest E, Van Aardenne J, Cooper OR, Kainuma M, Mahowald N, McConnell JR, Naik V, Riahi K, van Vuuren DP. Historical (1850–2000) gridded anthropogenic and biomass burning emissions of reactive gases and aerosols: methodology and application. Atmos Chem Phys 2010;10:7017–39. doi:10.5194/acp-10-7017-2010.

Lamarque JF, Emmons LK, Hess PG, Kinnison DE, Tilmes S, Vitt F, Heald CL, Holland EA, Lauritzen PH, Neu J, Orlando JJ, Rasch PJ, Tyndall GK. CAM-chem: description and evaluation of interactive atmospheric chemstiry in the Community Earth System Model. Geosci Model Dev 2012;5:369–411. doi:10.5194/gmd-5-369-2012.

Lamarque JF, Kyle GP, Meinshausen M, Riahi K, Smith SJ, van Vuuren DP, Conley AJ, Vitt F. Global and regional evolution of short-lived radiatively-active gases and aerosols in the representative concentration pathways. Clim Change 2011;109:191–212. doi:10.1007/s10584-011-0155-0.

Lawrence DM, Oleson KW, Flanner MG, Thornton PE, Swenson SC, Lawrence PJ, Zeng X, Yang ZL, Levis S, Sakaguchi K, Bonan GB, Slater AG. Parameterization improvements and functional and structural advances in version 4 of the Community Land Model. J Adv Model Earth Sys 2011;3. doi:10.1029/2011MS000045.

Mantua NJ, Hare SR, Zhang Y, Wallace JM, Francis RC. A Pacific interdecadal climate oscillation with impacts on salmon production. Bull Amer Meteor Soc 1997;78:1069–79.

Meinshausen M, Smith SJ, Calvin K, Daniel JS, Kainuma MLT, Lamarque JF, Matsumoto K, Montzka SA, Raper SCB, Riahi K, Thomson A, Velders GJM, van Vuuren DPP. The RCP greenhouse gas concentrations and their extensions from 1765 to 2300. Clim Change 2011;109:213–41. doi:10.1007/s10584-011-0156-z.

Mizuta R, Arakawa O, Ose T, Kusunoki S, Endo H, Kitoh A. Classification of CMIP5 future climate responses by the tropical sea surface temperature changes. SOLA 2014;10:167–71. doi:10.2151/sola.2014-035.

National Academies of Sciences, Engineering, and Medicine . Attribution of extreme weather events in the context of climate change. The National Academies Press, 2016. doi:10.17226/21852.

Neale RB, Chen CC, Gettelman A, Lauritzen PH, Park S, Williamson DL, Conley AJ, Garcia R, Kinnison D. Lamarque JF, Marsh D, Mills M, Smith AK, Tilmes S. Vitt F, Morrison H, Cameron-Smith P, Collins WD, Iacono MJ, Easter RC, Ghan SJ, Liu X, Rasch PJ, Taylor MA. Description of the NCAR community atmosphere model (CAM 5.0). Technical Report; NCAR Technical Note NCAR/TN-486+STR; 2012.

Oleson KW, Lawrence DM, Bonan GB, Flanner MG, Kluzek E, Lawrence PJ, Levis S, Swenson SC, Thornton PE, Dai A, Decker M, Dickinson R, Feddema J, Heald CL, Hoffman F, Lamarque JF, Mahowald N, Niu GY, Qian T, Randerson J, Running S, Sakaguchi K, Slater A, Stockli R, Wang A, Yang ZL, Zeng X, Zeng X. Technical description of version 4.0 of the Community Land Model (CLM). Technical Report NCAR Technical Note NCAR/TN-478+STR; National Center for Atmospheric Research; Boulder, CO, U.S.A.; 2010.

Pall P, Aina T, Stone DA, Stott PA, Nozawa T, Hilberts AGJ, Lohmann D, Allen MR. Anthropogenic greenhouse gas contribution to flood risk in England and Wales in Autumn 2000. Nature 2011;470:382–5.

Reynolds RW, Rayner NA, Smith TM, Stokes DC, Wang WC. An improved in situ and satellite SST analysis for climate. J Clim 2002;15:1609–25.

Risser MD, Stone DA, Paciorek CJ, Wehner MF, Angélil O. Quantifying the effect of interannual ocean variability on the attribution of extreme climate events to human influence. Clim Dyn 2017;doi:10.1007/s00382-016-3492-x.

Saji NH, Yamagata T. Possible impacts of Indian Ocean Dipole mode events on global climate. Climate Res 2003;25:151–69.

Schaller N, Kay AL, Lamb R, Massey NR, van Oldenborgh GJ, Otto FEL, Sparrow SN, Vautard R, Yiou P, Ashpole I, Bowery A, Crooks SM, Haustein K, Huntingford C, Ingram WJ, Jones RG, Legg T, Miller J, Skeggs J, Wallom D, Weisheimer A, Wilson S, Stott PA, Allen MR. Human influence on climate

in the 2014 southern England winter floods and their impacts. Nature Clim Change 2016;6:627–34. doi:10.1038/NCLIMATE2927.

Shepherd TG. A common framework for approaches to extreme event attribution. Curr Clim Change Rep 2016;2:28–38. 10.1007/s40641-016-0033-y.

Shiogama H, Imada Y, Mori M, Mizuta R, Stone D, Yoshida K, Arakawa O, Ikeda M, Takahashi C, Arai M, Ishii M, Watanabe M, Kimoto M. Attributing historical changes in probabilities of record-breaking daily temperature and precipitation extreme events. SOLA 2016;12:225–31. doi:10.2151/sola.2016-045.

Shiogama H, Watanabe M, Imada Y, Mori M, Kamae Y, Ishii M, Kimoto M. Attribution of the June-July 2013 heat wave in the southwestern United States. SOLA 2014;10:122–6. doi:10.2151/sola.2014-025.

Stone DA. A hierarchical collection of political/economic regions for analysis of climate extremes. Geosci Model Dev 2017;:Submitted.

Stone DA, Allen MR. The end-to-end attribution problem: from emissions to impacts. Clim Change 2005;71:303–18.

Stone DA, Christidis N, Folland C, Perkins-Kirkpatrick S, Perlwitz J, Shiogama H, Wehner MF, Wolski P, Cholia S, Krishnan H, Murray D, Angélil O, Beyerle U, Ciavarella A, Dittus A, Quan XW. Experiment design of the international clivar c20c+ detection and attribution project. Weather and Climate Extremes In preparation;.

Stone DA, Pall P. A benchmark estimate of the effect of anthropogenic emissions on the ocean surface. Geosci Model Dev 2017;:Submitted.

Stott PA, Allen M, Christidis N, Dole R, Hoerling M, Huntingford C, Pall P, Perlwitz J, Stone D. Attribution of weather and climate-related extreme events. In: Asrar GR, Hurrell JW, editors. Climate Science for Serving Society: Research, Modelling and Prediction Priorities. Springer; 2013. p. 307–37.

Stott PA, Mitchell JFB, Allen MR, Delworth TL, Gregory JM, Meehl GA, Santer BD. Observational constrains on past attributable warming and predictions of future global warming. J Climate 2006;19:3055–69.

Taylor KE, Stouffer RJ, Meehl GA. An overview of CMIP5 and the experiment design. Bull Amer Met Soc 2012;93:485–98.

Wang YM, Lean JL, Sheeley NRJ. Modeling the Sun's magnetic field and irradiance since 1713. Astrophys J 2005;625:522–38. doi:10.1086/429689.

Wehner M, Prabhat , Reed KA, Stone D, Collins WD, Bacmeister J. Resolution dependence of future tropical cyclone projections of CAM5.1 in the U.S. CLIVAR Hurricane Working Group idealized configurations. J Clim 2015;28:3905–25. doi:10.1175/JCLI-D-14-00311.1.

Wolski P, Stone D, Tadross M, Wehner M, Hewitson B. Attribution of floods in the Okavango Basin, Southern Africa. J Hydrol 2014;511:350–8.

Wolter K, Timlin MS. El/Niño Southern Oscillation behavior since 1871 as diagnosed in an extended multivariate ENSO index (MEI.ext). Int J Climatol 2011;31:1074–87.

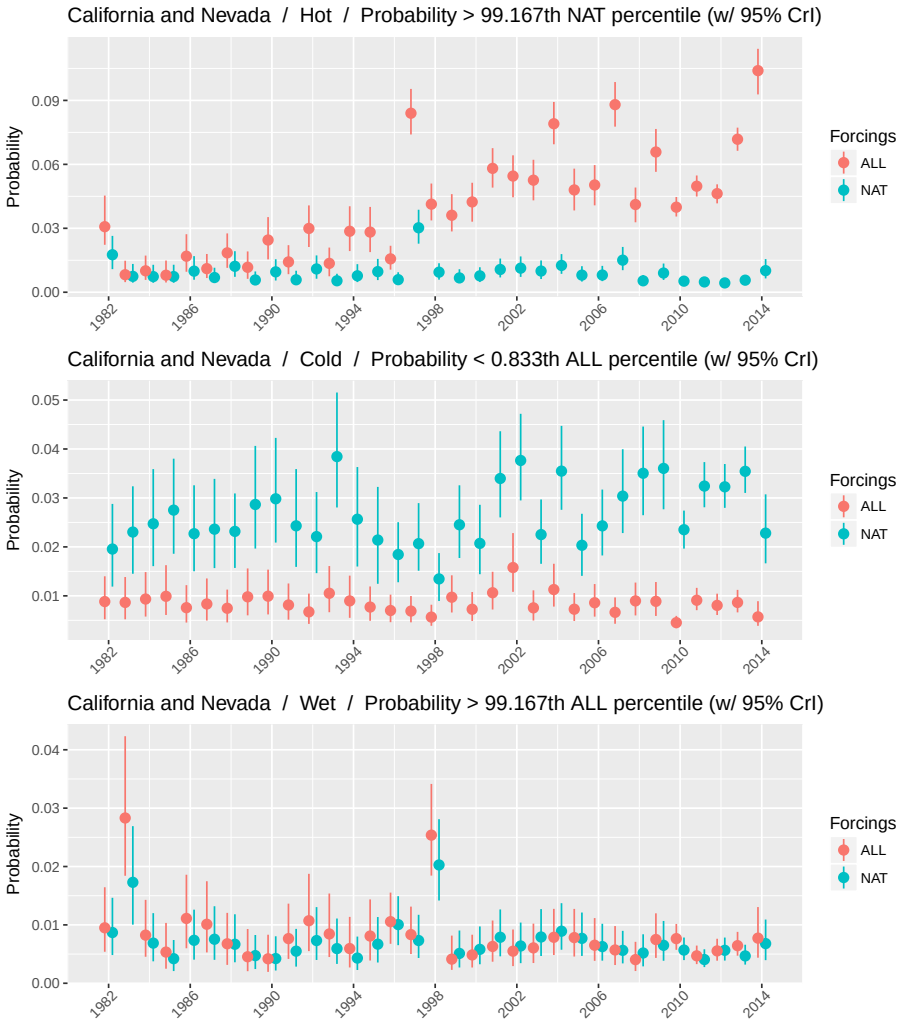

Figure 1: Time series of estimated probabilities of exceedence of a threshold for hot (top), cold (middle), and wet (bottom) months over the states of California and Nevada, U.S.A., for the All-Hist/est1/v2-0 simulations (red) and Nat-Hist/est1/v2-0 simulations (blue). The thresholds correspond to the 1-in-10-year event over the 1982-2014 period in the All-Hist/est1/v2-0 simulations.

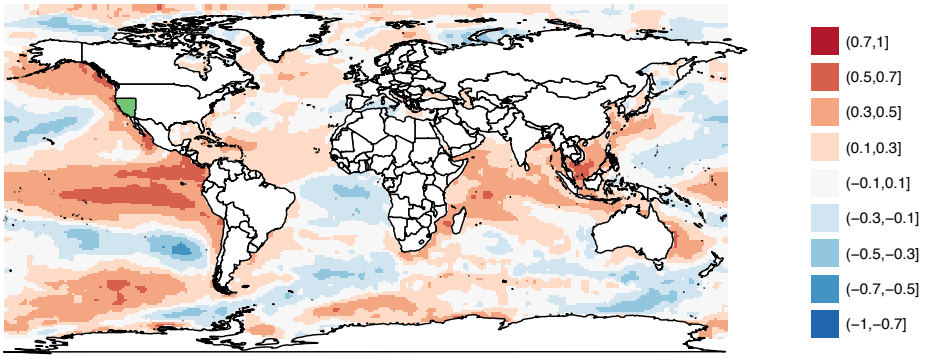

Figure 2: Map of the correlation of annual mean sea surface temperatures with the year-to-year variability (δ_t) in the risk ratio for wet months over the U.S. states of California and Nevada. δ_t is calculated from the CAM5.1-1degree simulations using the method of Risser et al. (2017). Sea surface temperature data are from Hurrell et al. (2008) updated with NOAA OI.v2 (Reynolds et al., 2002), the same data used by the All-Hist/est1/v2-0 simulations.

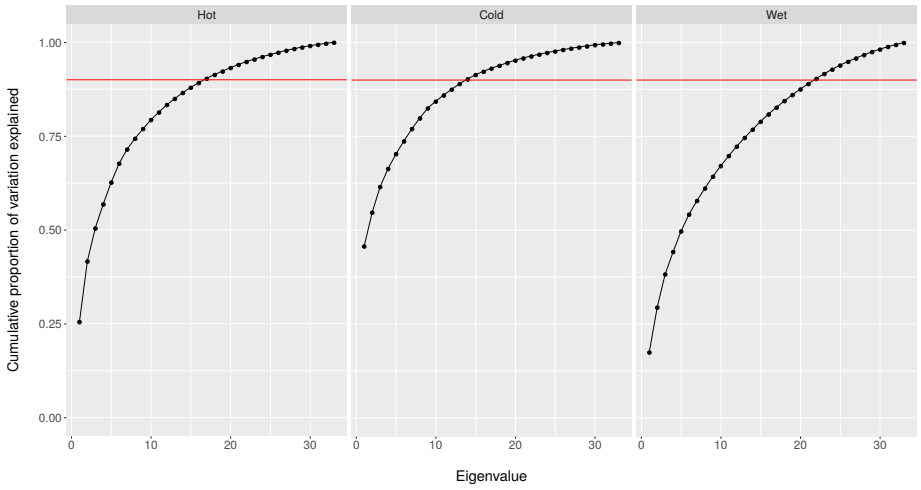

Figure 3: Cumulative proportion of the anomalous variation in the risk ratio across all 237 regions that is is represented by the given number of principal components, for hot (left), cold (middle), and wet (right) events. The point at which the curves cross the red line indicates the number of principals required to represent 90% of the anomalous variation in the risk ratio.

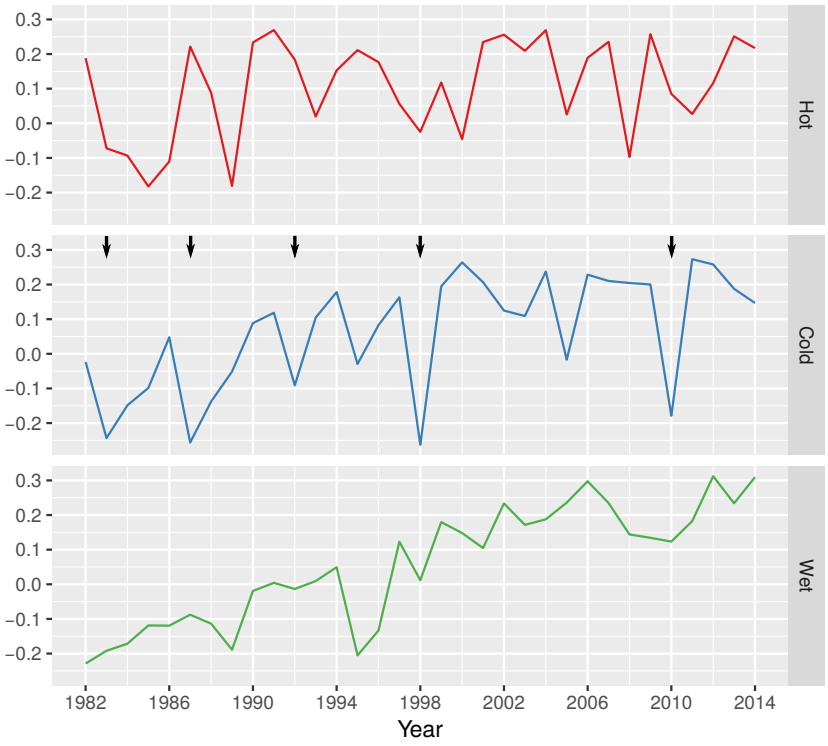

Figure 4: The time series of the leading principal component of the anomalous variation in the risk ratio across all 237 regions during the 1982–2014 period: hot events (top), cold events (middle), and wet events (bottom). Arrows in the cold events panel denote the strongest five El Niño events during the period as defined by the January-March Extended Multivariate ENSO Index (Wolter and Timlin, 2011).

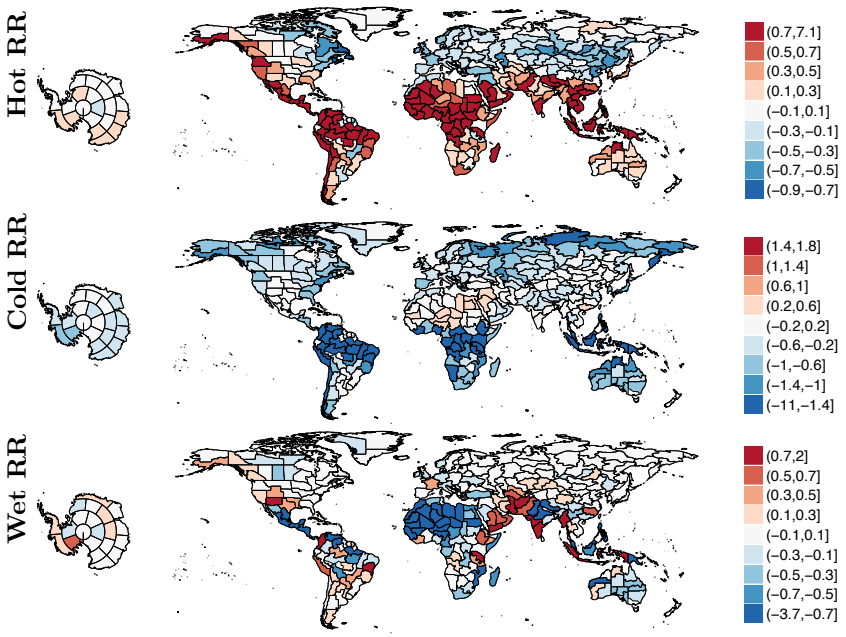

Figure 5: The spatial projection of the leading principle component of the anomalous variation in the risk ratio across all 237 regions during 1982-2014 period: hot events (top), cold events (middle), and wet events (bottom).

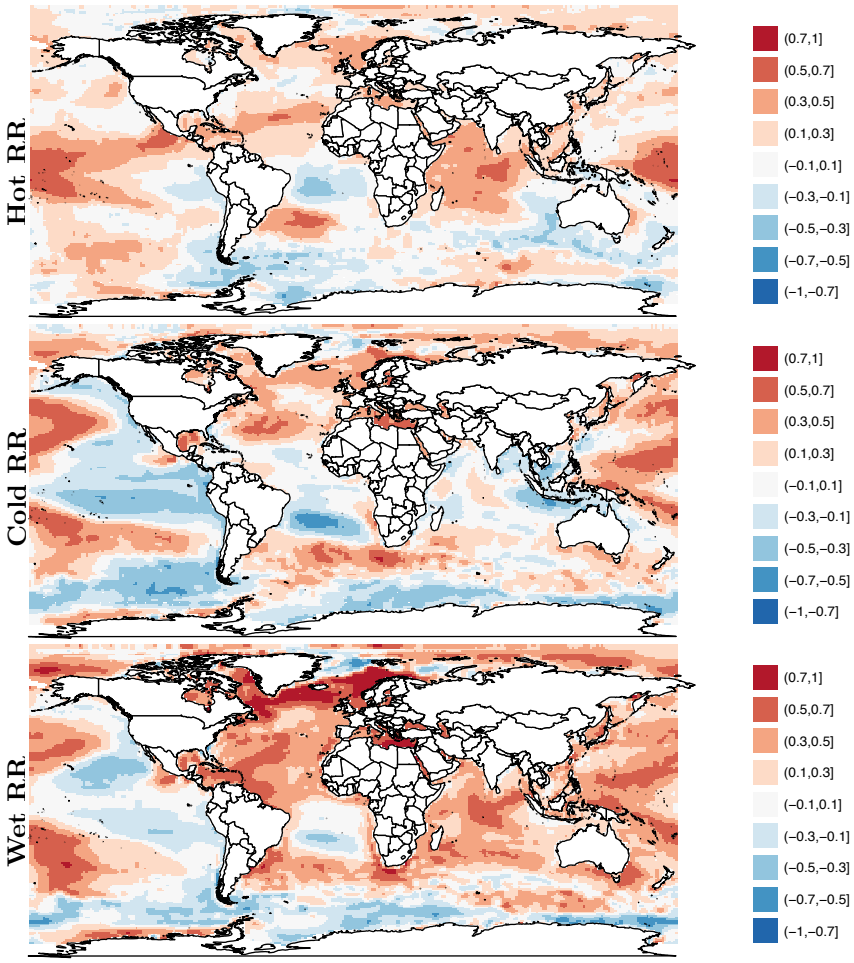

Figure 6: Correlation of the leading of principal component of anomalous variation in the risk ratio across all 237 regions against 1982–2014 sea surface temperatures for: hot events (top), cold events (middle), and wet events (bottom).